

Mergers of neutron star black hole binaries with small mass ratios: nucleosynthesis, gamma-ray bursts and electromagnetic transients

S. Rosswog¹

¹ School of Engineering and Science, International University Bremen, Germany

ABSTRACT

I discuss simulations of the coalescence of black hole neutron star binary systems with black hole masses between 14 and 20 M_{\odot} . The calculations use a three-dimensional smoothed particle hydrodynamics code, a temperature-dependent, nuclear equation of state and a multi-flavor neutrino scheme. General relativistic effects are mimicked using the Paczyński -Wiita pseudo-potential and gravitational radiation reaction forces.

Opposite to previous, purely Newtonian calculations, in none of the explored cases episodic mass transfer occurs. The neutron star is always completely disrupted after most of its mass has been transferred directly into the hole. For black hole masses between 14 and 16 M_{\odot} an accretion disk forms, large parts of it, however, are inside the last stable orbit and therefore falling with large radial velocities into the hole. These disks are (opposite to the neutron star merger case) thin and -apart from a spiral shock- essentially cold. For higher mass black holes ($M_{\text{BH}} \geq 18 M_{\odot}$) almost the complete neutron star disappears in the hole without forming an accretion disk. In these cases the surviving material is spun up by tidal torques and ejected as a half-ring of neutron-rich matter. None of the investigated systems is a promising GRB central engine. We find between 0.01 and 0.2 M_{\odot} of the neutron star to be dynamically ejected. Like in a type Ia supernova, the radioactive decay of this material will power a light curve with a peak luminosity of a few times 10^{44} erg/s. The maximum will be reached about three days after the coalescence and will be mainly visible in the optical/near infrared band. The coalescence itself may produce a precursor pulse with a thermal spectrum of ~ 10 ms duration.

Subject headings: gamma rays: bursts, stars: neutron, methods: numerical

1. Introduction

Neutron star binary systems have been recognized as potential central engines of gamma-ray bursts (GRBs) already two decades ago, they have been mentioned in Paczyński (1986)

and Goodman et al. (1987) and discussed in more detail by Eichler et al. (1989) (for a more complete bibliography we refer to existing reviews, e.g. Meszaros 2002 or Piran 2005). As a variant of the neutron star binary case Paczyński (1991) discussed systems containing a neutron star (NS) and a stellar mass black hole (BH) as a possible GRB engine. These days, such compact binary systems are considered the 'standard model' for the subclass of short gamma-ray bursts, that last typically for about 0.3 s (Kouveliotou et al. 1993). Most recently, on 9 May 2005 the first ever X-ray afterglow for a short (~ 30 ms), hard GRB (GRB050509b) has been detected (Bloom et al. 2005). Its tentative association with a nearby giant elliptical galaxy has been interpreted as an indication for a compact binary merger origin of this burst (Bloom et al. 2005, Lee et al. 2005b). While NSBH binaries are usually just considered to be a minor variation on the topic of double neutron star merger (DNS), it has been pointed out recently (Rosswog et al. 2004) that it is not obvious, that such a coalescence will automatically produce a hot and massive accretion disk around the hole. Therefore, its role for gamma-ray bursts needs further investigations.

During the disruption process tidal torques are expected to eject material into highly eccentric, possibly unbound orbits. This debris is extremely neutron rich, $Y_e \sim 0.1$, and therefore (if ejected at appropriate rates) holds the promise to be one of the still much debated sources of r-process elements (Lattimer and Schramm 1974 and 1976).

Moreover, NSBH systems are generally considered promising sources for ground-based gravitational wave detectors such as LIGO (Abramovici et al. 1992), GEO600 (Luck et al. 2001), VIRGO (Caron et al. 1997) and TAMA (Tagoshi et al. 2001).

It is worth pointing out in this context that there is a controversy about the rates at which NSBH mergers do occur. Bethe and Brown (1998) argued that NSBH should merge about an order of magnitude more frequently than DNS, while a recent study by Pfahl et al. (2005) comes to the conclusion that the number of NSBH systems in the Galaxy should be below 1 % of the number of double neutron star systems. To date 8 DNS have been observed (Stairs 2004), while not a single NSBH binary has been discovered yet.

Neutron star black hole merger simulations have been performed by several groups. Most of the simulations use Newtonian or pseudo-Newtonian gravity. Janka et al. (1999) used a grid based hydrodynamics code together with a nuclear equation of state (EOS) and a neutrino leakage scheme to explore the role of these mergers in GRB context. Lee (2000, 2001) and Lee and Kluzniak (1999a,b) used smoothed particle hydrodynamics with polytropic equations of state to explore the sensitivity of the results to the adiabatic exponent of the EOS. Lee and Ramirez-Ruiz (2002) have analyzed the flow pattern within an accretion disk around a BH and, in recent papers (Lee and Ramirez-Ruiz 2004, Lee et al. 2005), they included detailed microphysics in their simulations. Setiawan et al. (2004) constructed disks around stellar mass black holes and followed their evolution including explicit viscosity, Rosswog et al. (2004) investigated the dynamics of the accretion process. It is worth pointing out that

both Setiawan et al. (2004) and Lee et al. (2005) implicitly assume that interesting disks form whose properties they subsequently investigate whereas the focus of this investigation is the question whether/what kind of a disk forms during the merger.

Recently, there has been progress in the relativistic treatment black hole neutron star binaries. Taniguchi et al. (2005), for example, have been constructing quasi-equilibrium black hole neutron star binaries in general relativity, and further efforts with approximate relativistic treatments seem to be underway (Rasio et al. 2005).

Stellar mass black holes formed in core collapse supernovae are thought to be born with masses ranging from about 3 to 20 M_{\odot} (Fryer and Kalogera 2001). Numerical simulations have so far only explored black hole masses up to 14 M_{\odot} (Janka et al. 1999 and Lee and Kluzniak 1999a,b and Lee 2000, 2001 used black holes up to 10 M_{\odot} , Rosswog et al. 2004 explored masses up to 14 M_{\odot}). In this paper we will focus on black holes with masses ranging from 14 to 20 M_{\odot} . The 14 M_{\odot} case has been explored previously (Rosswog et al. 2004) using the same microphysics but a purely Newtonian BH-potential and may therefore serve to gauge the effect of the Paczyński -Wiita pseudo-potential.

A simple estimate for the radius where a star around a BH is disrupted is the tidal radius, $R_{\text{tid}} = \left(\frac{M_{\text{BH}}}{M_{\text{NS}}}\right)^{1/3} R_{\text{NS}}$. As it grows slower with the black hole mass ($\propto M_{\text{BH}}^{1/3}$) than the gravitational radius ($\propto M_{\text{BH}}$), it is expected that higher mass BHs will have more difficulties building up massive disks. Therefore, the lower end of the black hole mass distribution is most promising for the launch of a GRB. Unfortunately, it is very difficult to find suitable approximations for these cases, as here the space-time is far from a static Schwarzschild/Kerr solution and therefore neither the use of pseudo-potentials nor solving the hydrodynamics equations in a fixed background metric are admissible. For these cases fully dynamical general relativistic calculations are needed.

In this paper we will explore the accretion dynamics and the observational signatures of the high mass end of these binary systems.

2. Simulations

We use a 3D smoothed particle hydrodynamics code that has been developed to simulate compact objects. Most of the code features have been described elsewhere (Rosswog et al. 2000, Rosswog and Davies 2002, Rosswog and Liebendörfer 2003) and will only be briefly mentioned for the sake of completeness. For the simulations described here we have changed to an integration scheme with individual time steps and also the treatment of the black hole is different from the previous implementation.

In our implementation we have taken particular care to avoid artifacts from the use of artificial viscosity. The quantities α and β that are usually used as fixed parameters in the artificial

viscosity tensor (Monaghan and Gingold 1983), are made time dependent and evolved by solving an additional differential equation (Morris and Monaghan 1997). In the absence of shocks $\alpha = \alpha^* = 0.1$ (we always use $\beta(t) = 2 \cdot \alpha(t)$), to be compared with the ‘standard values’ of $\alpha = 1$ and $\beta = 2$. In strong shocks our α is allowed to rise up to values of 2 in order to avoid post-shock oscillations (Rosswog et al. 2000). In addition, the Balsara prescription (Balsara 1995) is used to avoid spurious forces in pure shear flows. Thus, artificial viscosity is essentially absent unless a shock is detected. These measures have proved very effective, suppressing unwanted effects of artificial viscosity by orders of magnitude (Rosswog et al. 2000; Rosswog and Davies 2002).

We use a temperature-dependent nuclear equation of state that is based on the tables provided by Shen et al. (1998a, 1998b) and that has been smoothly extended to the low-density regime (Rosswog and Davies 2002). It covers a density range in $\log(\rho)$ from 0.5 to 15.4, temperatures from 0 to 100 MeV and electron fractions, Y_e , from 0 to 0.5. The nucleons are treated in the framework of temperature-dependent relativistic mean field theory. At densities below about 1/3 of nuclear matter density nuclei will be present in the plasma. Its composition is determined for fixed ρ , T and Y_e from an equilibrium of nucleons, alpha particles and an average heavy nucleus. Thus, energy release due to nuclear transmutations is accounted for in a simple way. Contributions of photons and electrons/positrons of arbitrary degree of relativity and degeneracy are added to the thermodynamic quantities. Details can be found in Rosswog and Davies 2002.

Nowhere (apart from the initial neutron stars) β -equilibrium is assumed. Local changes in the electron fraction and the thermal energy content of matter due to neutrinos are accounted for with a multi-flavor neutrino treatment (Rosswog and Liebendörfer 2003).

The Newtonian self-gravity of the neutron star fluid is calculated using a binary tree (e.g. Benz et al. 1990). This makes the star less compact and might -at least quantitatively- influence the accretion process. We use a Paczyński -Wiita potential to approximately take into account the presence of general relativistic effects around the black hole such as the presence of a last stable orbit. Clearly, the use of the Paczyński -Wiita potential is not a complete substitute for fully fledged general relativistic hydrodynamic simulations around a Schwarzschild black hole. It has, however, turned out to be astonishingly accurate: test-particle orbits with $r < 6 M_{\text{BH}}$ (geometrical units with $G=c=1$ are used throughout the paper) are unstable and orbits with $r < 4 M_{\text{BH}}$ are unbound, i.e. the radius of marginally stable orbit is located at $R_{\text{isco}} = 6 M_{\text{BH}}$, and the radius of the marginally bound orbit is $R_{\text{mb}} = 4 M_{\text{BH}}$. Direct comparisons with general relativistic solutions in a Schwarzschild space time show that the pseudo-potential is able to capture the essentials of general relativity and can reproduce accretion disk structures to an accuracy of better than 10 % (see e.g. Artemova et al. 1996). The pseudo-potential does, however, not prevent velocities from becoming larger than unity. Abramowicz et al. (1996) have suggested a rescaling of the velocities found

using Newtonian models together with the Paczyński -Wiita potential (i.e. in our case the numerical velocities): $v_{\text{num}} = v_{\text{phys}} \cdot \tilde{\gamma}$, where $\tilde{\gamma} = (1 - (v_{\text{phys}})^2)^{-1/2}$. They found this rescaling to reproduce the exact relativistic velocities to better than 5 %. This could be used, for example, to calculate Doppler shifts, this rescaling is however nowhere used in this paper.

The build up of the binary tree from scratch is computationally expensive, therefore we do not remove the particles that have crossed our inner boundary (located at $R_{\text{bd}} = 3 M_{\text{BH}}$) at each time step. They are only removed when a dump is written, i.e. every $2.5 \cdot 10^{-5}$ s which is as short as 1/12 of the neutron star dynamical time scale and therefore does not lead to any artifacts (this has been confirmed by removing particles every time step). To avoid numerical problems with the singularity of the Paczyński -Wiita potential we have extended it smoothly with a polynomial (see Appendix A and Fig. 12). Note that all particles that have ever encountered a deviation from the Paczyński -Wiita potential inside R_{bd} will be removed at the next dump.

We have implemented two different time integration schemes with individual time steps: a second-order Runge-Kutta-Fehlberg method (Fehlberg 1968) and a second-order predictor-corrector scheme. Both of these schemes have been tested extensively against a Runge-Kutta-Fehlberg scheme with a global time step. As the results were nearly indistinguishable the simulations were run with the predictor-corrector method as it only requires one force evaluation per time step. The most time consuming part of these simulations is the inspiral where (due to the stiff neutron star EOS and the resulting flat stellar density profile) practically all particles have to be evolved on the shortest time step. The gain in speed for the presented calculations is moderate (factors of a few), but in other test problems the code was faster by more than two orders of magnitude.

We construct our initial neutron stars by solving the Lane-Emden-equations for our EOS with the additional constraint of (cold) β -equilibrium. This yields stellar radii of about 16 km for a $1.4 M_{\odot}$ neutron star. All SPH-particles have the same mass to avoid numerical noise arising from interactions of particles with unequal masses. Prior to setting up the binary system the neutron stars are relaxed carefully by applying an additional, velocity proportional damping forces in the equations of motion so that the SPH-particles can settle into their equilibrium positions. Once such an equilibrium is obtained the NS-BH-binary system is set up, either with a tidally locked or a non-spinning neutron star. The locked systems are constructed accurately using the hydrocode itself (see Rosswog et al. 2004). The non-spinning neutron stars are set on orbit with an angular frequency determined by the force balance between centrifugal and gravitational forces. In all cases the radial velocity component of a point mass binary of the considered separation is added.

The simulations presented here use up to $3 \cdot 10^6$ SPH particles and are currently the best resolved models of neutron star black hole encounters (Rosswog et al. (2004) used up to 10^6 particles, Lee (2001) used slightly more than 80000 particles).

3. Results

3.1. Merger dynamics

The dynamics of the coalescence is illustrated in Figures 1 and 3, movies can be found at <http://www.faculty.iu-bremen.de/srosswog/movies.html>. In all of the cases the neutron star is completely disrupted after a large portion of its mass has been transferred directly into the hole. The corresponding peak accretion rates exceed $1000 M_{\odot}/s$ for about 1 ms, after this short episode they drop by at least two orders of magnitude, see panel one in Figure 4. It is instructive to compare the $14 M_{\odot}$ case to the corresponding case of our previous study (Rosswog et al. 2004), where we had used a Newtonian BH potential. In the purely Newtonian case we found episodic mass transfer with a low-mass, “mini neutron star” surviving throughout the whole simulation or about eight close encounters. In the Paczyński -Wiita case about $1.15 M_{\odot}$ (see panel two in Figure 4) are transferred directly into the hole, the rest forms a rapidly expanding tidal tail. The tidal tail still contains an outward-moving density maximum (corresponding to the mini neutron star of the Newtonian case), but its self-gravity is not strong enough to form a spherical object. The results are well converged, runs I and II show excellent agreement in the BH masses and peak mass transfer rates. Some minor deviations are visible at low mass transfer rates (see panel one in Fig. 4 and the distance, R_{MT} , where numerically resolvable mass transfer sets in; see column seven in Table 1).

The case with $16 M_{\odot}$ BHs behaves qualitatively very similar to the $14 M_{\odot}$ BHs: slightly more mass (about $1.2 M_{\odot}$) is transferred into the hole, the disk is slightly less massive, hot and dense than the $14 M_{\odot}$ case. Again, the two different resolutions yield nearly identical results.

The systems containing BHs of $18 M_{\odot}$ or more (runs V, VI and IX) do not form accretion disks at all. Almost the complete neutron star flows via the inner Lagrange point directly into the hole, only a small fraction of the star is spun up enough by tidal torques to be dynamically ejected, see last column in Table 2. In these cases the remnant consists of the black hole (without any accretion disk) and a rapidly expanding, concentric (half-)ring of neutron-rich debris material ($0.08 M_{\odot}$ for the 18 and $0.01 M_{\odot}$ for $20 M_{\odot}$ BH), see Figure 3. The result that it seems to be intrinsically difficult to form promising accretion disks (at least for the investigated mass ratios) is consistent with recent estimates of Miller (2005).

Table 1: Summary of the different runs. M_{BH} : black hole mass in solar units; $q=M_{\text{NS}}/M_{\text{BH}}$; ns spin: C= tidally locked, I= non-spinning neutron star; R_{tid} : tidal radius; a_0 : initial separation; R_{isco} : last stable orbit Schwarzschild black hole; R_{MT} : distance where numerically resolvable mass transfer sets in; all radii are given in units of km; # part.: SPH particle number; T_{sim} : simulated duration in ms.

run	M_{BH}/q	ns spin	R_{tid}	a_0	R_{isco}	R_{MT}	# part.	T_{sim}
I	14/0.1	C	36.1	127.5	124.1	117	570587	34.6
II	14/0.1	C	36.1	127.5	124.1	125	2971627	40.8
III	16/0.0875	C	37.7	145.5	141.8	122	570587	78.1
IV	16/0.0875	C	37.7	145.5	141.8	123	1005401	60.9
V	18/0.0778	C	39.3	162.0	159.6	123	570587	50.4
VI	20/0.07	C	40.7	187.5	177.3	128	1503419	179.6
VII	14/0.1	I	36.1	126.2	124.1	116	1497453	49.8
VIII	16/0.0875	I	37.7	143.9	141.8	121	1497453	39.8
IX	18/0.0778	I	39.3	160.4	159.6	126	1497453	205.4

Table 2: Results the different runs. M_{BH} : black hole mass in solar units; $q=M_{\text{NS}}/M_{\text{BH}}$; $a_{\text{BH}} = J_{\text{BH}}/M_{\text{BH}}^2$ is the dimensionless black hole spin parameter at the end of the simulation (J_{BH} : angular momentum transferred into the hole); $L_{\nu,\text{tot}}^{\text{peak}}$ is the peak luminosity (ers/s) of the sum of all neutrino flavors; M_{ej} refers to the material (in solar masses) that is dynamically ejected during the merger; $E_{\text{kin,ej}}$: kinetic energy in ejecta (erg) at end of simulation.

run	M_{BH}/q	a_{BH}	$L_{\nu,\text{tot}}^{\text{peak}}$	M_{ej}	$E_{\text{kin,ej}}$
I	14/0.1	0.196	$8 \cdot 10^{50}$	0.20	$2.7 \cdot 10^{52}$
II	14/0.1	0.200	$8 \cdot 10^{50}$	0.20	$2.8 \cdot 10^{52}$
III	16/0.0875	0.197	$3 \cdot 10^{50}$	0.15	$2.1 \cdot 10^{52}$
IV	16/0.0875	0.197	$2 \cdot 10^{50}$	0.15	$2.1 \cdot 10^{52}$
V	18/0.0778	0.201	$< 10^{46}$	0.08	$1.3 \cdot 10^{52}$
VI	20/0.07	0.198	$< 10^{46}$	0.01	$2.2 \cdot 10^{51}$
VII	14/0.1	0.203	$1 \cdot 10^{51}$	0.17	$2.2 \cdot 10^{52}$
VIII	16/0.0875	0.206	$6 \cdot 10^{49}$	0.11	$1.3 \cdot 10^{52}$
IX	18/0.0778	0.207	$< 10^{46}$	0.04	$5.6 \cdot 10^{51}$

3.2. Disk structure

A hot and thick accretion disk around a black hole is believed to be an essential ingredient for a GRB. As described in the previous section, and as expected from simple analytical estimates, more promising disks form for larger mass ratios, i.e. smaller BH masses. In the described simulations only systems with BH masses below $18 M_{\odot}$ form an accretion disk at all. In the following the most promising case, run II ($M_{\text{BH}} = 14 M_{\odot}$, tidal locking), is discussed, the $q = 0.1$ case with a non-rotating neutron star (run VII) looks very similar. In those cases where a disk forms, substantial parts of it are inside the innermost stable circular orbit at $R_{\text{isco}} = 6 M_{\text{BH}}$, and are therefore “plunging” with large radial velocities towards the hole which leads to a substantial consumption of the disks during the simulated time. For illustration, Fig. 5 shows the distribution of the SPH-particles at $t = 18.396$ ms of run II. Shown are the projections of the particles onto the orbital (=XY-) plane (black) and overlaid are the projections to the XZ-plane of those particles j with $|y_j| < 150$ km (red) to show the vertical disk structure. Moreover the locus of the Schwarzschild radius and R_{isco} are shown. While the matter cross section far away from the hole is close to circular, the disk close to the hole is geometrically thin ($|z| \ll \bar{\omega} = \sqrt{x^2 + y^2}$) apart from the region close to the spiral shock where the accretion stream interacts with itself. In this regions the disk is slightly puffed up. Due to the plunge motion only moderate densities ($\log(\rho) < 10.5 \text{ g cm}^{-3}$) and temperatures are reached (see Fig. 6). The disk is essentially cold apart from the spiral shock where the temperatures reach ~ 2.5 MeV.

The geometrically thin, relatively cool disks that we find for black hole masses between 14 and $16 M_{\odot}$ is in stark contrast to the thick disks that form in the neutron star merger case (see Figs. 15 and 16 in Rosswog and Davies (2002)).

3.3. Neutrino emission

The annihilation of neutrino anti-neutrino pairs is one possibility to deposit energy in the baryon free region above the hole. In the cases with black hole masses $\geq 18 M_{\odot}$ the neutrino emission negligible ($< 10^{46}$ erg/s). The most promising cases are, as expected, the ones with the lowest black hole masses. If disks form at all they are completely transparent to the emerging neutrinos. In lowest mass cases with $M_{\text{BH}} = 14 M_{\odot}$ (runs I, II, and VII) we find peak luminosities of $L_{\nu, \text{tot}} = L_{\nu_e} + L_{\bar{\nu}_e} + L_{\nu_x} \approx 10^{51}$ erg/s (where the index x refers to the heavy lepton neutrinos), i.e. our most promising cases here yield luminosities that are more than two orders of magnitude smaller than in our neutron star merger calculations where the same microphysics was used. The average energies of the emitted neutrinos are between 12 and 15 MeV. Opposite to the neutron star merger case the neutrino luminosity

does not settle into a stationary state, since the disk is being consumed on a time scale of tens of milliseconds. In the tidally locked case we find a single neutrino pulse of about 20 ms duration, in the case without neutron star spin we find two neutrino pulses separated by about 15 ms, see Figure 7.

4. Summary and Discussion

We have performed three-dimensional hydrodynamic simulations of neutron black hole encounters with mass ratios $q = \frac{M_{\text{ns}}}{M_{\text{BH}}} \leq 0.1$. We used a state-of-the-art temperature-dependent, nuclear EOS, a detailed, multi-species neutrino treatment and the Paczyński - Wiita pseudo-potential.

We consider all the approximations made to be valid to a high degree. If an accretion disk forms at all (i.e. for the BH masses $< 18 M_{\odot}$) it is of only moderate density ($\sim 10^{10} \text{ g cm}^{-3}$) and completely transparent to neutrinos. Therefore the neutrino emission results cannot be influenced by the flux-limited diffusion treatment. Moreover, the results are numerically converged, different numerical resolutions yield almost identical results. The BHs are massive enough to dominate the space-time completely and as they are spun up to spin parameters of only 0.2 (see Table 2), we consider the use of PW-potentials a very good approximation (note that for $a=0.2$ the event horizon moves from 2 to 1.98 and the last stable orbit from 6 to 5.33 gravitational radii; see Fig. 8).

4.1. Implications for nucleosynthesis

The ejected mass fraction found in these simulations is generally *very* large (see Table 2), but comparable to the analytical estimates of Lattimer and Schramm (1974 and 1976), who estimated $0.05 \pm 0.05 M_{\odot}$. We had performed previously nucleosynthetic calculations for the decompressed ejecta in the neutron star merger case (Freiburghaus et al. 1999). As these calculations did not account for Y_e -changes due to weak interactions, Y_e was treated as a free parameter and was varied in a range that is reasonable for neutron star material (0.05 to 0.20). For values between 0.08 and 0.15 we found an almost perfect agreement with the observed, solar system r-process abundances from around Barium up to beyond the platinum peak. The value of Y_e has basically two effects: i) it determines the neutron to seed ratio and thus the maximum nucleon number A of the resulting abundance distribution and ii) the location of the reactions in the N-Z-plane, the so-called r-process path, which is, in this case, very close to the neutron drip-line. This path determines the nuclei that are involved and therefore the nuclear energy release and the corresponding β -decay time

scales. The initial neutron star material will be decompressed via the expansion and will therefore continuously change its composition. Starting from very large initial nuclei with hundreds of nucleons (the details of which are determined by the distributions of density, temperature and electron fraction) these transmutations will release nuclear binding energy until a final, β -stable composition has been reached. Figure 9 shows the snapshot distribution of Y_e within the debris of run II at $t = 18.396$ ms, in Figure 10 Y_e has been binned with the ejecta mass for the NSBH cases with $q=0.1$. Generally, as the only parts that have ever reached high temperatures disappear very quickly into the hole (see Fig. 6), the Y_e of the ejected material reflects closely its initial value inside the neutron star. The found Y_e s are generally very close to what was found in the neutron star merger case to give excellent results (compare Freiburghaus et al. 1999, Fig. 4; note, however, that due to the somewhat different expansion velocities, the interesting Y_e values may be slightly different in the NSBH case). To determine the exact elemental yields from these mergers is beyond the scope of the current work and is left to future investigations.

For the neutron star merger case Argast et al. (2004) found that a conflict with the observed element ratios in metal-poor halo stars may arise if neutron star mergers were the *dominant* r-process source. Similar questions may be raised for the NSBH case. One possibility to avoid the problem could be that NSBH coalesce much less frequently than DNS. This would be consistent with the non-observation of any NSBH-system (currently 8 DNS systems are known, see Stairs 2004) and the result of recent studies (Pfahl et al. 2005) that estimate the NSBH number in the Galactic disk to be less than 0.1-1% of the number of DNS.

We want to point out, however, that the ejecta found in our simulations exhibit very large radial velocities of $\approx 0.5c$. As most neutron star black hole binaries are expected to merge in the outskirts of galaxies (see e.g. Perna and Belczynski 2002) the chances are large that these high-velocity ejecta do not end up within the host galaxies, but rather enrich the intergalactic medium with very heavy, probably high-mass r-process elements. This interesting issue definitely requires further consideration in the future.

4.2. Gamma-ray Bursts

The formation of a massive accretion disk around a black hole is thought to be a vital ingredient for a GRB central engine. None of the systems investigated in this study yields disks that are promising as GRB engines. As the tidal radius only grows $\propto M_{\text{BH}}^{1/3}$ while the gravitational radius of the BH scales $\propto M_{\text{BH}}$, low mass black holes will easier form promising disks. In the simulations presented here, disks only form for BHs with masses below $18 M_{\odot}$. As mentioned previously, these disks are essentially cold apart from a spiral shock with temperatures of ≈ 2.5 MeV. Contrary to the neutron star merger case, these disks are

geometrically *thin*, of only moderate density and completely transparent to neutrinos. The peak densities in the shock are $\log(\rho) \approx 10.5$ (cgs) and lower elsewhere (see Fig. 6). This is to be compared with peak values of $\log(\rho) \approx 12$ (cgs) and $T \approx 4$ MeV in the neutron star merger case (Rosswog and Davies 2002). Moreover, the disk is drained substantially on the simulation time scale of a few 10 ms.

In the most promising cases the peak luminosities are about 10^{51} erg/s (see Table 2, Fig. 7). This is more than two orders of magnitude below the typical neutron star merger case (Rosswog and Liebendörfer, 2003). The hot debris of a double neutron star coalescence deposits $\sim 10^{48}$ erg/s via $\nu\bar{\nu}$ -annihilation in baryon-devoid regions and drives in this way a relativistic, bipolar outflow (Rosswog and Ramirez-Ruiz 2002, Aloy et al. 2005). The surrounding baryonic material collimates these jets into a small fraction of the solid angle so that they appear as isotropized $\sim 10^{50}$ erg (Rosswog and Ramirez-Ruiz 2003). As the neutrino annihilation rate scales roughly with the neutrino luminosity squared, the most promising cases of this study ($q=0.1$) will provide $L_{\text{jet,NSBH}} \approx 3 \cdot 10^{48} \cdot \left(\frac{10^{51}}{2 \cdot 10^{53}}\right)^2$ erg/s $\approx 10^{43}$ erg/s for about 10 ms. This estimate is rather on the optimistic side as, due to the thin disk geometry in the NSBH case, the probability for neutrinos to collide close to head-on (where the annihilation cross-section is maximal) is severely reduced. Moreover, such disks will not provide powerful winds from neutrino ablation to collimate a possible outflow. Therefore, the signal resulting from neutrino annihilation may be even less luminous. General relativistic effects like the bending of neutrino trajectories and the redshift of the neutrino energy may influence the result, but their influence goes in opposite directions and will change the non-relativistic results by only a factor of about two (Asano and Fukuyama 2001). Recently, Ramirez-Ruiz and Socrates (2005) have argued that neutrino spectra substantially different from black body may increase the overall explosion efficiency by more than an order of magnitude. But even if we stretch all of the available parameters to their most optimistic limits, e.g. assuming one order of magnitude more efficiency from neutrino spectra and an (ad hoc) extremely small beaming fraction $\zeta = \Omega/2\pi \sim 10^{-3}$, it is hard to see how the apparent isotropized luminosity should exceed, say, 10^{47} erg/s (for about 10 ms) even in the most promising cases of this study.

Another agent that can possibly feed energy into collimated outflow is the magnetic field. Being naturally endowed by strong magnetic fields to start with the shredding of a neutron star could be expected to be a good candidate for magnetic field amplification. This may occur via various pathways, the fastest of which is probably the magneto-rotational instability (Velikhov 1959, Chandrasekhar 1991, Balbus and Hawley 1998 and references therein). Fig. 11 shows the evolution of the disk-averaged magnetic field,

$$\langle B^{\text{eq}} \rangle = \sqrt{8\pi} \frac{\sum_i m_i \sqrt{\rho_i} c_{s,i}}{\sum_i m_i} \quad (1)$$

making the extreme assumption that the field can reach equipartition field strength. Here, the index i runs over the particles inside 600 km (see Figure 5) around the hole, m_i are the masses, ρ_i the densities and $c_{s,i}$ the sound velocities of the SPH-particles. Under this assumption an average field strength slightly in excess of 10^{14} G would result. Making the most optimistic assumptions, we will estimate the properties of the possibly resulting fireball (see Piran 1999 for a fireball review). The fireball energy is $E \sim \frac{(B^{\text{eq}})^2}{8\pi} V_{\text{ISCO}} \approx 4 \cdot 10^{48} \text{erg} B_{14}^2 \left(\frac{M_{\text{BH}}}{15M_{\odot}}\right)^3$. This yields an initial fireball temperature of $T_0 \approx 3.3 \text{ MeV} \left(\frac{E}{4 \cdot 10^{48} \text{erg}}\right)^{1/4} \left(\frac{M_{\text{BH}}}{15M_{\odot}}\right)^{-3/4}$. The critical value η_b , where $\eta = E/M$ with E and M energy and mass of the fireball, is given by (Piran 1999), $\eta_b \approx 6000 \left(\frac{E}{4 \cdot 10^{48} \text{erg}}\right)^{1/3} \left(\frac{M_{\text{BH}}}{15M_{\odot}}\right)^{-2/3}$. Given the fact that the resulting disk is very thin and neutrino ablation not important, we consider it plausible that the fireball is in the electron opacity dominated range, $\eta_b < \eta < \eta_{\text{pair}} \approx 5 \cdot 10^8 \left(\frac{E}{4 \cdot 10^{48} \text{erg}}\right)^{1/2} \left(\frac{M_{\text{BH}}}{15M_{\odot}}\right)^{-1/2}$. The fireball will thus become transparent to photons before it reaches the matter dominated stage. As the Lorentz-factor grows $\gamma \propto R$ and the fireball temperature drops $T \propto 1/R$, the observed temperature, $T_{\text{obs}} \propto \gamma T$, will be that of the initial fireball. This will yield a black body gamma-ray pulse with a temperature of about 3.3 MeV. Performing similar estimates for the fireball from neutrino annihilation yields a thermal pulse of about 2 MeV. SWIFT will have difficulties to detect it, but GLAST should be able to see a pulse of several tens of milliseconds out to a redshift of $z \sim 0.1$.

As mentioned previously, these estimates are based on most optimistic assumptions. As the material plunges into the hole within about one orbit once it has passed R_{ISCO} , any instability will have difficulties to amplify the field by large factors. The expected thermal precursor pulse may therefore be even weaker than estimated above.

In summary, none of the investigated systems seems to be an obvious candidate for the central engine of the observed short-hard GRBs. Neutron star black hole mergers may still be able to produce GRBs. Obviously, smaller mass black holes are more promising. Technically, however, they are much more challenging as the neutron star has a mass comparable mass to the black hole and space-time is far from the Schwarzschild solution. Therefore, neither the use of pseudo-potentials nor simulations on a fixed background space-time are justified, here fully relativistic 3D simulations of the full merger process are required.

The spin of the black hole may provide a possibility to launch GRBs even from more massive black holes. If they are spinning very rapidly from the beginning and are spun up further during the merger to values close to the maximum spin parameter of $a = 1$ then both the position of the last stable orbit and of the event horizon move to $1 M_{\text{BH}}$, see Fig. 8. Therefore, much higher temperatures and densities can be reached in the inner disk regions. The fraction of viable GRB candidates among the NSBH systems obviously depends on their mass and initial BH spin distribution. Both quantities are not observationally known and their predictions via population synthesis models are plagued by large uncertainties. It is

however clear, that not the whole available parameter space will provide conditions that are favorable to launch GRBs. This fact and the non-observation of even a single neutron star black hole system (while eight double neutron star systems are observed) makes it plausible that the observed short-hard GRBs are dominated by double neutron star coalescences.

4.3. Electromagnetic transients

In the investigated NSBH mergers we find very large amounts of radioactive material being ejected. The radioactive decay of this debris material would, like in a type Ia supernova, power the post-coalescence lightcurve. The bulk of ejecta material stems from the initial nucleon fluid of the neutron star and will end up in large, possibly r-process, nuclei. If we assume a typical nuclear binding energy of ~ 8 MeV per nucleon for the final nuclei, the decompression of this material will release, depending on the mass ratio of the NSBH system, between $\sim 1.6 \cdot 10^{50}$ and $\sim 3.2 \cdot 10^{51}$ erg from radioactive decays. The details of the resulting lightcurve will depend on the nuclear binding energies and decay time scales and their competition with the expansion of the material. As these nuclei will be extremely neutron rich (see Fig. 10) and far away from the valley of β -stability no experimental data for their half-lives are available and one would have to resort to theoretical predictions. For a simple estimate of the resulting electromagnetic transient from these radioactive ejecta we use the simple analytical estimate of Li and Paczyński (1998) who assumed spherical symmetry and a uniform distribution of nuclear lifetimes in logarithmic time intervals. Scaling their results with the numbers found in our simulations we find that the peak luminosity of $\sim 6 \cdot 10^{44}$ erg/s should be reached about 3 days after the coalescence (the 'banana-like' geometry may lead to a peak that occurs somewhat later than in the spherical model of Li and Paczyński). The effective temperature at peak will be $\sim 10^4$ K and result in an intensity maximum in the optical/near infrared band of the spectrum.

It is, however, worth pointing out that this result relies on radioactive nuclei still being present when the ejecta become optically thin, which depends on the details of the nuclear reaction path. It may also be possible that the decays have ceased already by that time and the result is an essentially 'dark explosion'. This interesting topic definitely deserves further examination.

In summary, the merger of a neutron star with a black hole of a mass beyond $14 M_{\odot}$ may, rather than producing a gamma-ray burst, yield a supernova-like transient with a thermal precursor pulse peaking in the gamma-ray band. Such a precursor of ~ 10 ms duration should be detectable with GLAST out to a redshift of $z \sim 0.1$. Follow-up observations should then be able to detect a few days later the supernova-like transient.

Movies of the simulations can be found under
<http://www.faculty.iu-bremen.de/srosswog/movies.html>.

It is a pleasure to thank Marek Abramowicz, Jim Lattimer, William Lee, Andrew MacFadyen, Enrico Ramirez-Ruiz, Roland Speith and Christophe Winisdoerffer for useful discussions and the INFN in Catania and the IAS in Princeton for their hospitality. The calculations reported here have been performed on the JUMP supercomputer of the Höchstleistungsrechenzentrum Jülich.

Appendix A: Paczyński -Wiita potential with smooth extension

Here we show the form of the potential that is used in the simulations. To numerically avoid the singularity at the Schwarzschild-radius we extend the Paczyński -Wiita acceleration denominator, $D_{\text{PW}} = \frac{1}{(r-R_s)^2}$, smoothly down to vanishing radius with a polynomial, D_{pol} , that possesses the following properties:

i) it matches D_{PW} at a transition radius, R_t : $D_{\text{PW}}(R_t) = D_{\text{pol}}(R_t)$,

ii) the derivatives match smoothly: $\frac{dD_{\text{PW}}}{dr}(R_t) = \frac{dD_{\text{pol}}}{dr}(R_t)$,

iii) its derivative vanishes in the origin $\frac{dD_{\text{pol}}}{dr}(0) = 0$.

Using $A = R_t^{-1} \cdot (R_s - R_t)^{-3}$ and $B = \frac{R_s - 2R_t}{(R_s - R_t)^3}$ the force denominator is expressed as

$$D = \begin{cases} Ar^2 + B & \text{for } r < R_t \\ \frac{1}{(r-R_s)^2} & \text{for } r \geq R_t. \end{cases}$$

The form of D is shown in Fig. 12, we always use $R_t = 3 M_{\text{BH}}$. Note that every particle that has ever been inside R_t is removed at the next dump step (the time between two subsequent dumps is a small fraction ($\approx 1/12$) of the neutron star dynamical time).

REFERENCES

- Abramovici A., Althouse W. E., Drever R. W. P., Gursel Y., Kawamura S., Raab F. J., Shoemaker D., Sievers L., Spero R. E., Thorne K. S., Science, 256, 325 (1992)
- Abramowicz, M.A., Beloborodov, A.M., Chen, X.M. and Ithumenshchev, I.V., A&A, 313, 334 (1996)
- Argast, D., Samland, M., Thielemann, F.-K. and Qian, Y.-Z., A&A, 416, 997 (2004)
- Asano, K. and Fukuyama, T., ApJ, 546, 1019 (2001)
- Balbus, S.A. and Hawley, J.F., Rev. Mod. Phys., 70, 1 (1998)
- Balsara D., J. Comput. Phys., 121, 357 (1995)
- Benz W., Bowers R., Cameron A., Press W., 1990, ApJ, 348, 647
- Bloom, J.S. et al., astro-ph/0505480 (2005)
- Chandrasekhar, S., Proc. Nat. Acad. Sci USA, 46, 53 (1960)
- Fehlberg, E., NASA Technical Report TR-R287 (1968)
- Janka, H.-T., Eberl, T., Ruffert, M., Fryer, C.L., ApJ, 527, L39 (1999)
- Lattimer, J. and Schramm, D.N., ApJ, 192, L145 (1974)
- Lattimer, J. and Schramm, D.N., ApJ, 210, L549 (1976)
- Lattimer, J. et al., ApJ, 213, L225 (1977)
- Lee, W.H. and Kluzniak, W.L., ApJ, 526, 178 (1999)
- Lee, W.H. and Kluzniak, W.L., MNRAS, 308, 780 (1999)
- Lee, W.H., MNRAS, 318, L606 (2000)
- Lee, W.H., MNRAS, 328, 583 (2001)
- Lee, W.H., Ramirez-Ruiz, E. and Page, D., astro-ph/0506121 (2005)
- Lee, W.H., Ramirez-Ruiz, E. and Granot, J., astro-ph/0506104 (2005)
- Miller, M.C., astro-ph/0505094 (2005)
- Morris J., Monaghan J., J. Comp. Phys., 136, 41 (1997)

- Novikov, I.D. and Frolov, V.P., *Physics of Black Holes*, Dordrecht: Kluwer (1989)
- Perna, R. and Belczynski, K., *ApJ*, 570, 252 (2002)
- Pfahl, E., Podsiadlowski, P. and Rappaport, S., *astro-ph/0502122*
- Piran, T., *Phys. Rep.*, 314, 575 (1999)
- Ramirez-Ruiz, E. and Socrates, A., *astro-ph/0504/257* (2005)
- Rasio, F., Faber, J., Kobayashi, S. and Laguna, P., *astro-ph/0503007* (2005)
- Rosswog S., Davies M. B., Thielemann F.-K., Piran T., *A & A*, 360, 171 (2000)
- Rosswog, S. and Davies, M.-B., *MNRAS*, 334, 481 (2002)
- Rosswog, S. and Ramirez-Ruiz, E. *MNRAS*, 336, L7 (2002)
- Rosswog, S. and Liebendörfer, M., *MNRAS*, 342, 673 (2003)
- Rosswog, S., Ramirez-Ruiz, E. and Davies, M.B., *MNRAS* 345, 1077 (2003)
- Rosswog, S. and Ramirez-Ruiz, E., *MNRAS*, 343, L36 (2003)
- Setiawan, S., Ruffert, M., Janka, H.-T., *MNRAS*, 352, 753 (2004)
- Shen H., Toki H., Oyamatsu K., Sumiyoshi K., *Nuclear Physics, A* 637, 435 (1998)
- Shen H., Toki H., Oyamatsu K., Sumiyoshi K., *Prog. Theor. Phys.*, 100, 1013 (1998)
- Stairs, I.H., *Science*, 304, 547 (2004)
- Taniguchi, K., Baumgarte, T.W., Faber, J.A. and Shapiro, S.L., *astro-ph/0505450v2* (2005)
- Velikhov, E.P., *Sov. Phys. JETP.*, 36, 995 (1959)

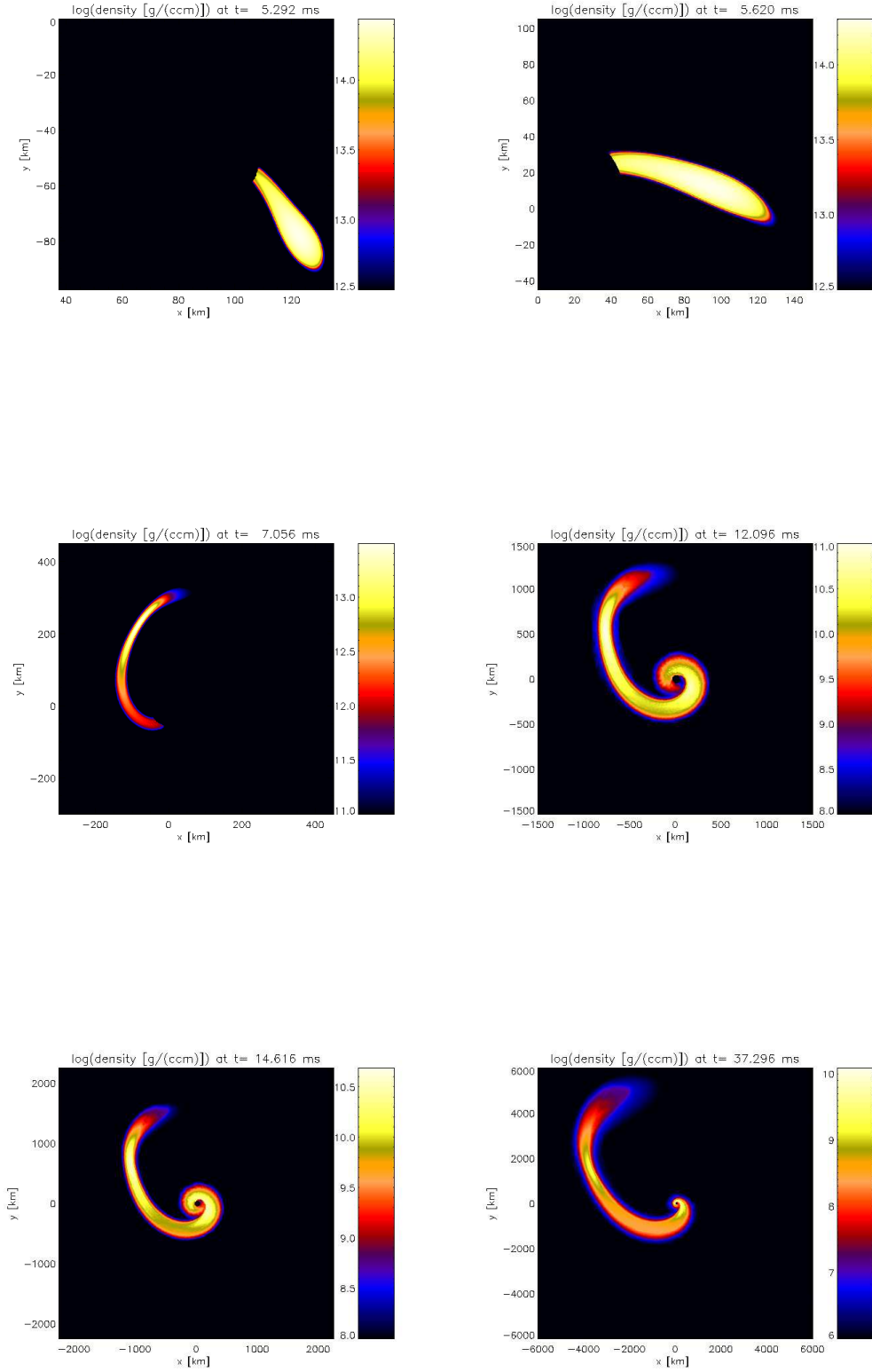


Figure 1: Evolution of the density perturbation for $\text{Re}(\omega) = 0.1$ (initially $\log(\rho) = 12.5$)

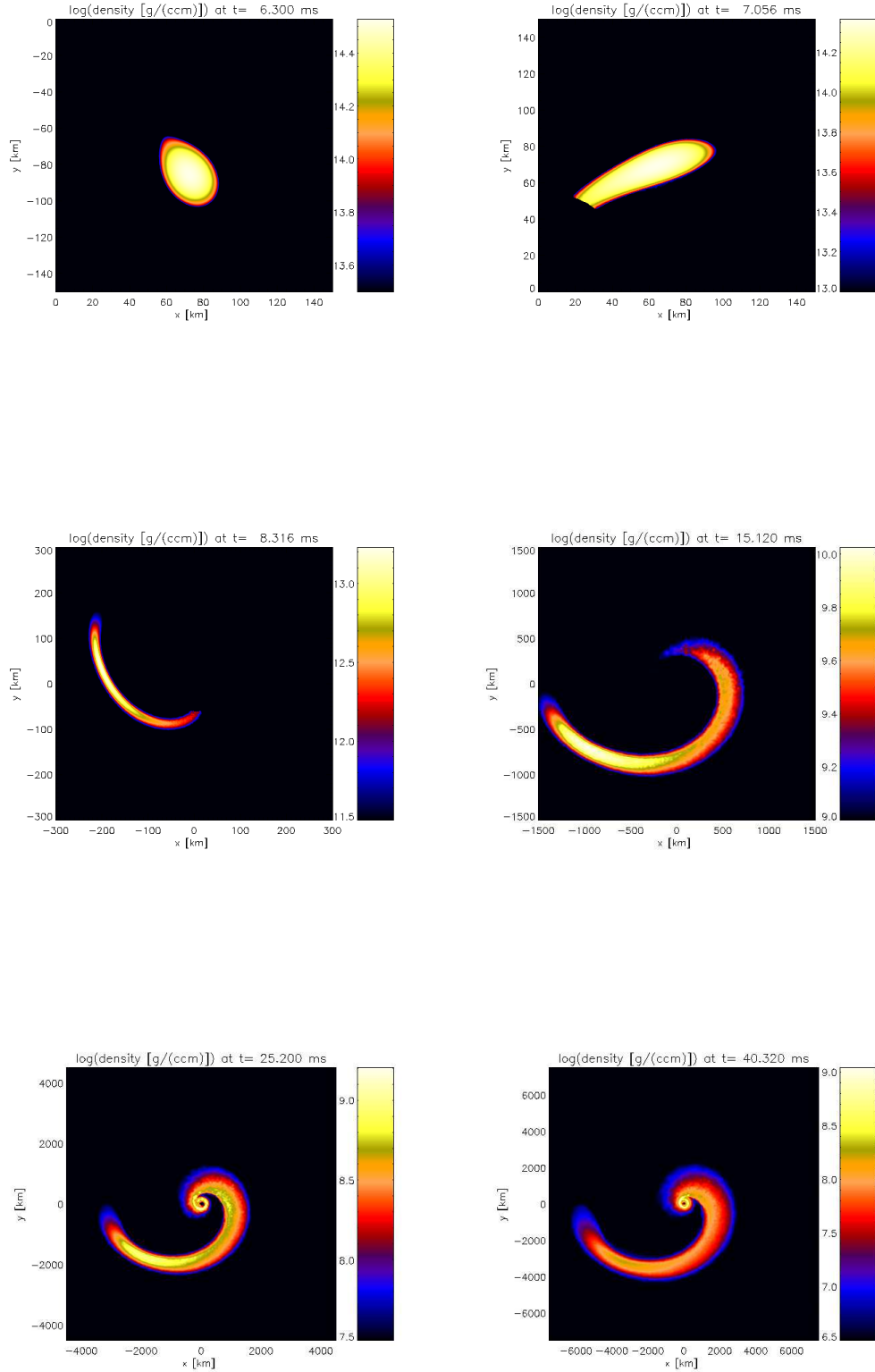


Figure 9: Density distribution of $\text{D}_{\text{IV}}(\alpha = 0.9875)$ (left column) at $t = t_{\text{IV}}$.

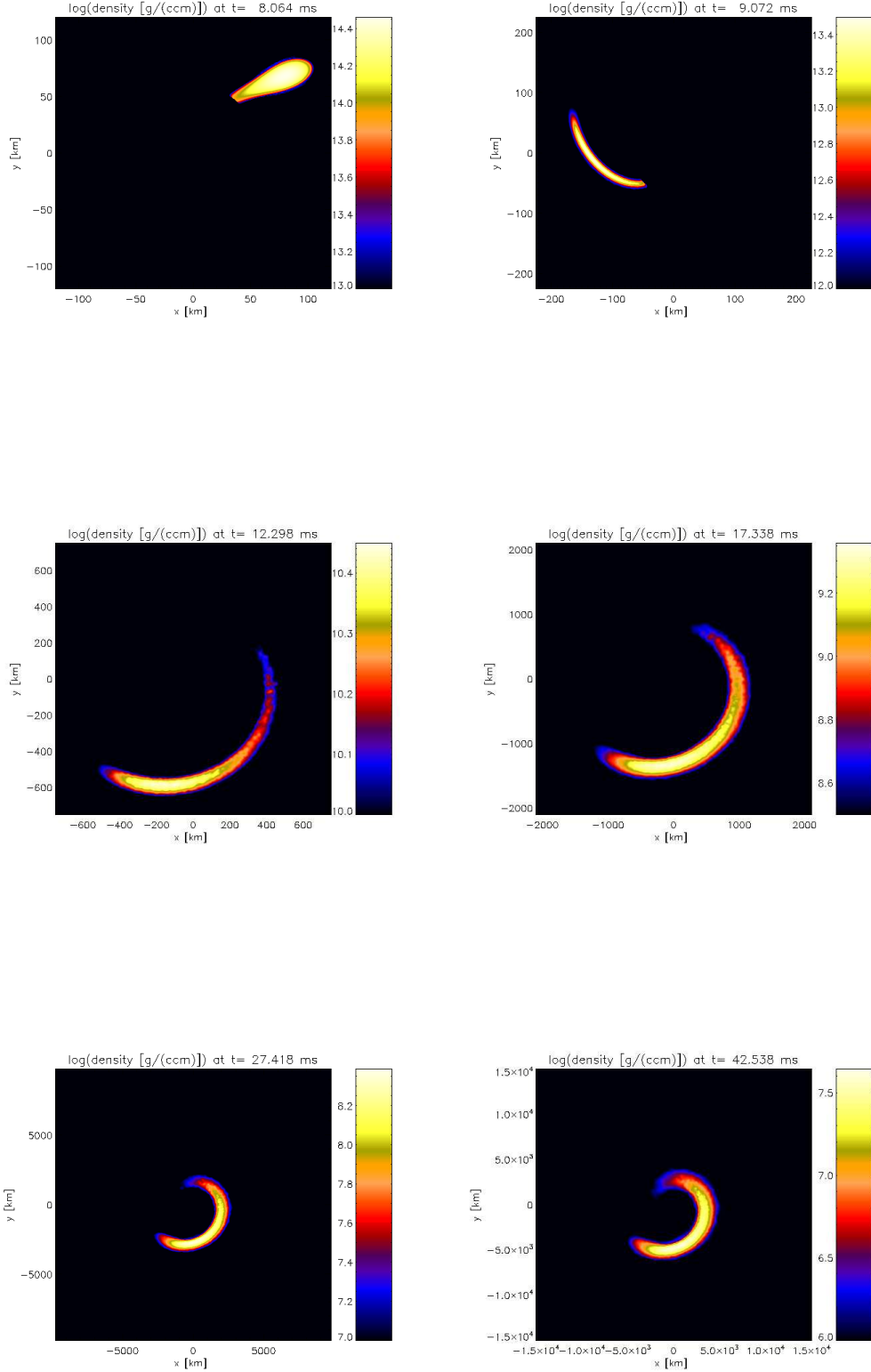


Figure 2: Density in the orbital plane of $D_{\text{max}} = 0.0778$ (filled black) at $t = t_0$.

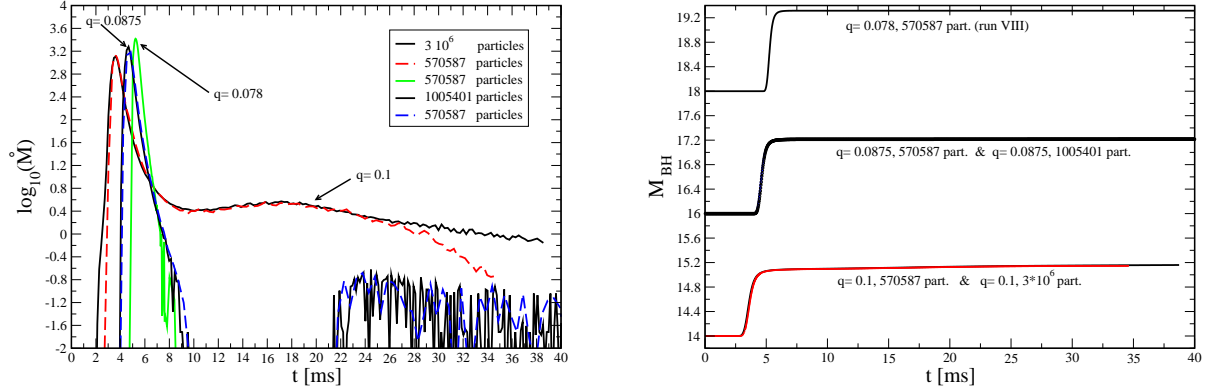


Fig. 4.— Left panel: The mass transfer rates as a function of time. In one case ($q=0.078$, i.e. $M_{\text{BH}}=18 M_{\odot}$) the mass transfer stops completely. This is also true for the $20 M_{\odot}$ case (not shown). Right panel: The growth of the black hole with time is shown for five of the runs. Note that the runs that simulate the same systems (run I and II; run III and IV) with different resolutions yield nearly identical curves.

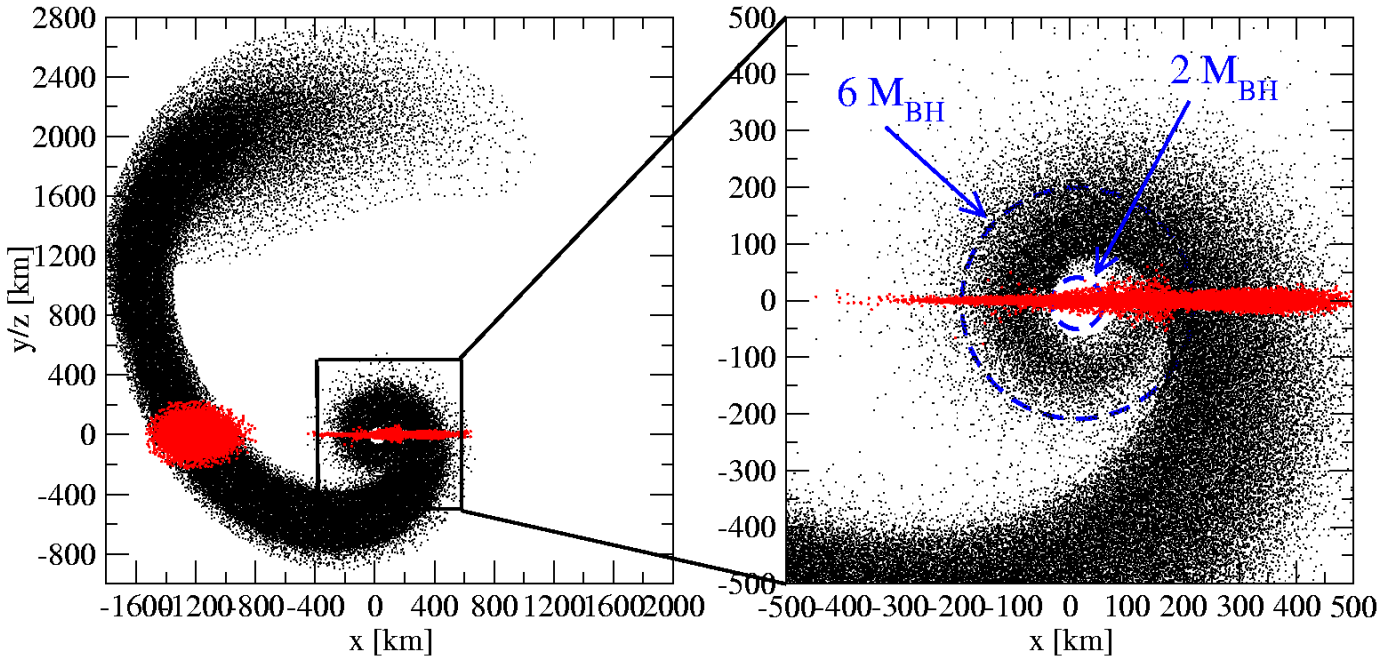


Fig. 5.— Shown are the projections of the SPH particle positions onto the orbital plane (run II at $t=18.396$ ms). Overlaid are the projections to the X-Z-plane of those particles with $|y_i| < 150$ km and the positions of the Schwarzschild-radius and the innermost stable circular orbit of a test particle around a Schwarzschild black hole. In regions of high column number densities only a fraction of the particles are displayed.

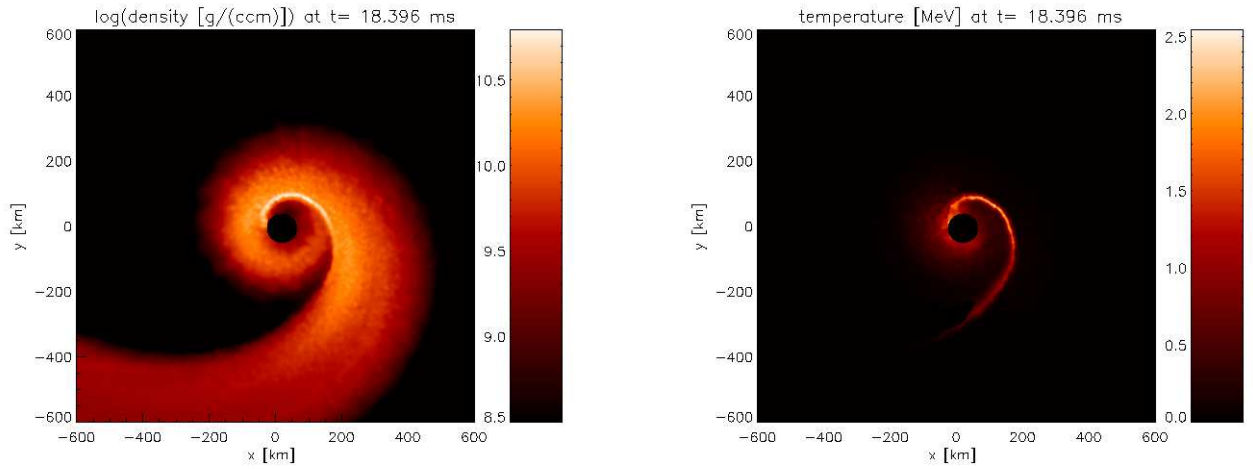


Fig. 6.— Blow-up of the inner disk region of run II at $t=18.396$ ms after simulation start (left panel: $\log(\text{density})$; right panel: temperature). Clearly visible are the shock, where the accretion stream interacts with itself.

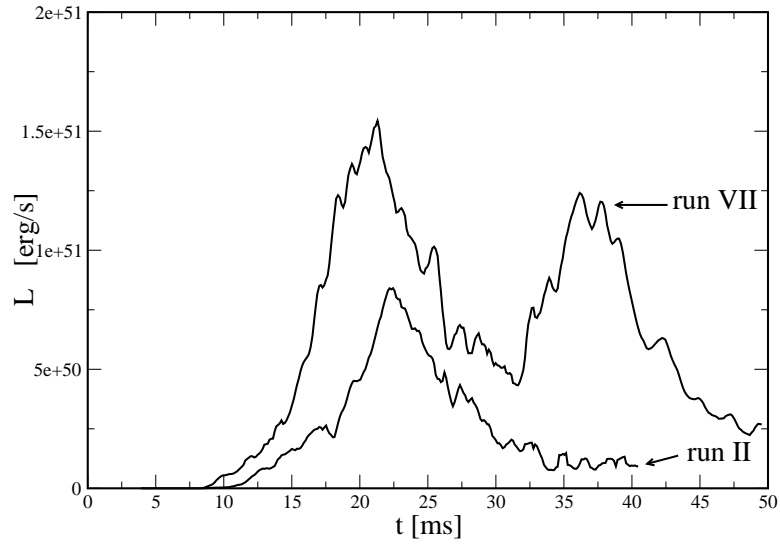


Fig. 7.— Shown are the total neutrino luminosities of runs II ($q= 0.1$, tidal locking) and run VII ($q= 0.1$, no neutron star spin).

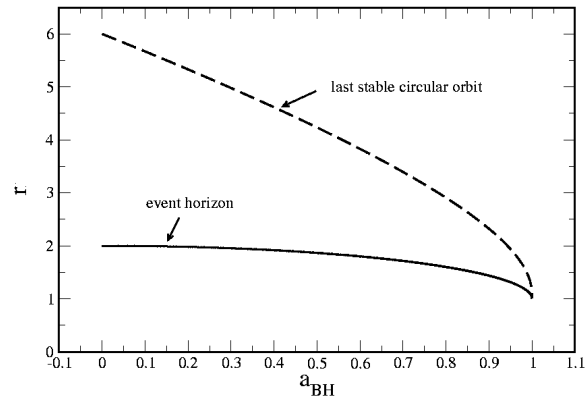


Fig. 8.— Position of the event horizon and the last stable circular orbit around a spinning black hole (see Novikov and Frolov 1989) as a function of the spin parameter $a_{\text{BH}} = J_{\text{BH}}/M_{\text{BH}}^2$.

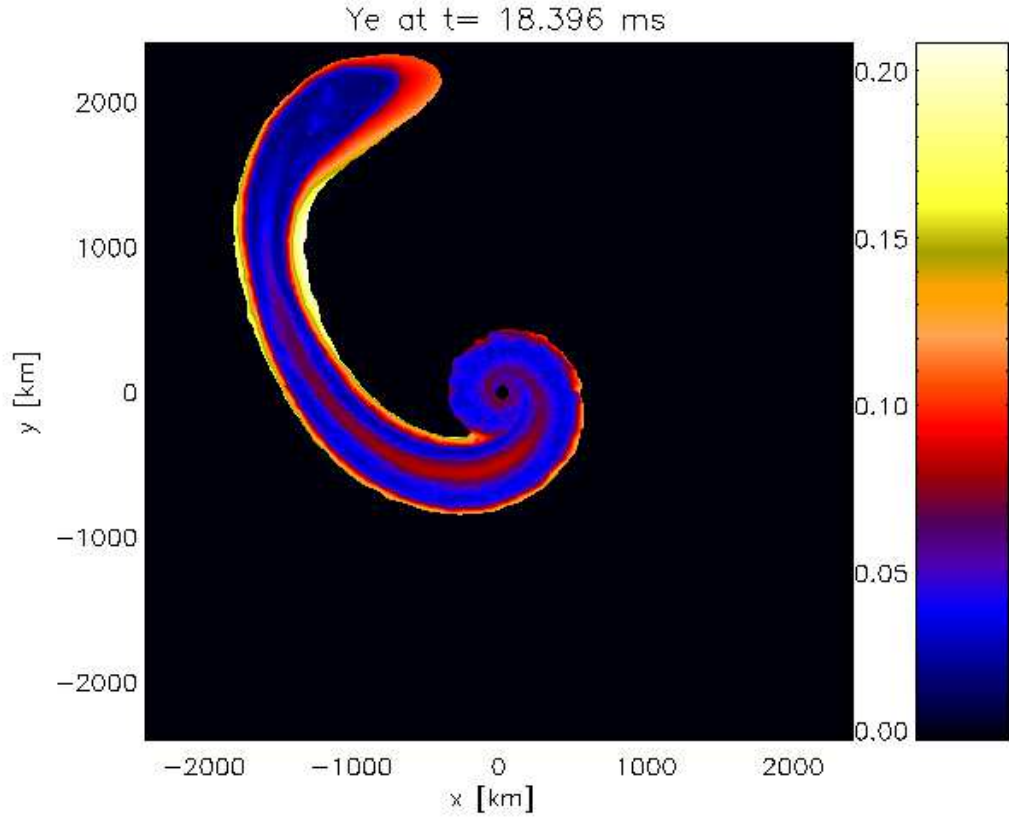


Fig. 9.— Electron fraction, Y_e , in the orbital plane (run II, $q= 0.1$, tidal locking). The high- Y_e skin around the remnant is the initial neutron star crust.

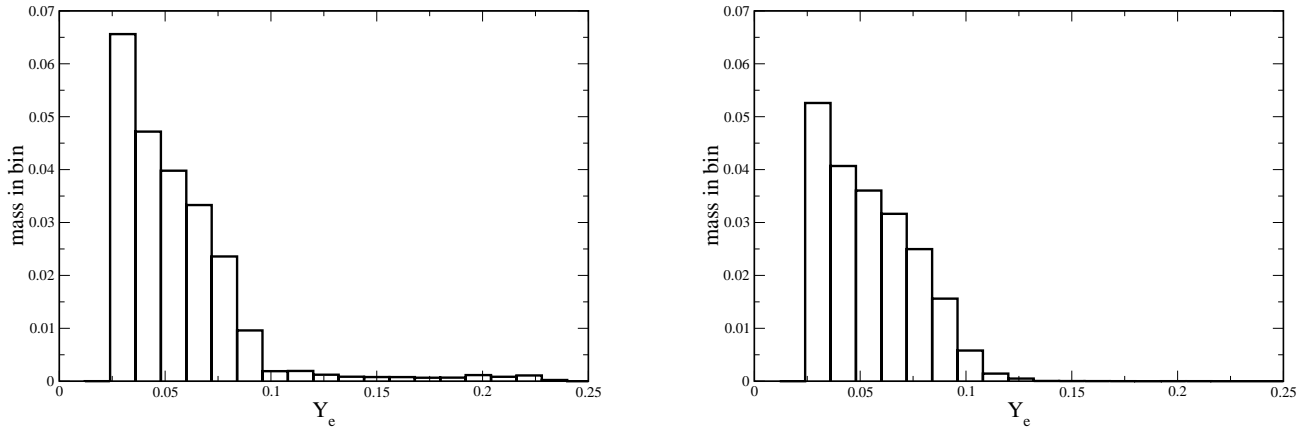


Fig. 10.— Histogram of the ejected mass binned according to Y_e . The left panel refers to run II ($q=0.1$, tidal locking), the right one to run VII ($q=0.1$, no neutron star spin). The missing high- Y_e tail in the right panel may be an effect of the somewhat lower numerical resolution.

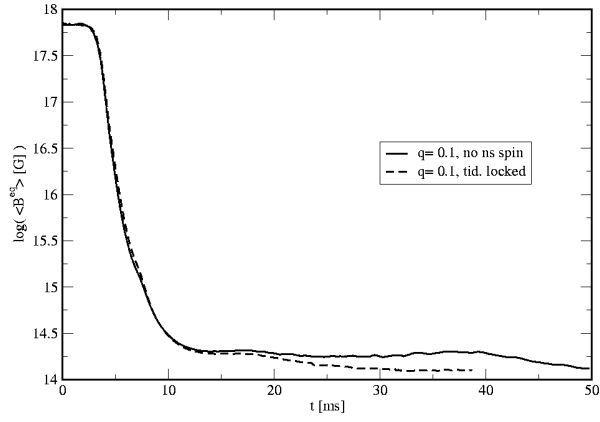


Fig. 11.— Shown are the equipartition field strengths for run II ($q= 0.1$, tidal locking; dashed line) and run VII ($q= 0.1$, no neutron star spin; solid line) of the neutron star material averaged over the innermost 600 km (“disk”) as a function of time.

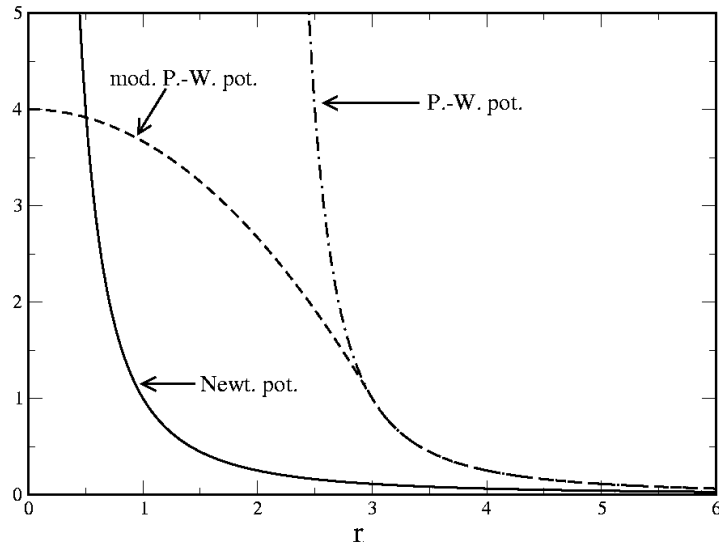


Fig. 12.— Comparison of the denominator for purely Newtonian, Paczyński -Wiita and modified Paczyński -Wiita forces introduced to avoid the singularity at $2 M_{\text{BH}}$ (for a transition radius, $R_t = 3M_{\text{BH}}$; see Appendix for details). All particles that have ever been inside R_t are removed.